DENTAL MATERIALS 35 (2019) 403–413

Available online at www.sciencedirect.com

ScienceDirect

journal homepage: www.intl.elsevierhealth.com/journals/dema

Hydrophobicity of graphene as a driving force for inhibiting biofilm formation of pathogenic bacteria and fungi

Shruti Vidhawan Agarwalla[a], *Kassapa Ellepola*[a], *Mariana Caldeira Ferraz da Costa*[b], *Guilhermino José Macêdo Fechine*[b], *Julien Luc Paul Morin*[c], *A.H. Castro Neto*[c], *Chaminda Jayampath Seneviratne*[a], *Vinicius Rosa*[a,c,*]

[a] *Faculty of Dentistry, National University of Singapore, Singapore*
[b] *Graphene and Nanomaterials Research Centre, MackGraphe, Mackenzie Presbyterian University, Brazil*
[c] *Centre for Advanced 2D Materials and Graphene Research Centre, National University of Singapore, Singapore*

ARTICLE INFO

Article history:
Received 28 May 2018
Received in revised form
18 September 2018
Accepted 26 September 2018

Keywords:
Peri-implantitis
Coating
Implant
Candida albicans
Carbon
Infection
Surface free energy
Wettability
Roughness
Graphene

ABSTRACT

Objective. To evaluate the surface and wettability characteristics and the microbial biofilm interaction of graphene coating on titanium.

Methods. Graphene was deposited on titanium (Control) *via* a liquid-free technique. The transfer was performed once (TiGS), repeated two (TiGD) and five times (TiGV) and characterized by AFM (n = 10), Raman spectroscopy (n = 10), contact angle and SFE (n = 5). Biofilm formation (n = 3) to *Streptococcus mutans*, *Enterococcus faecalis*, *Pseudomonas aeruginosa* and *Candida albicans* was evaluated after 24 h by CV assay, CFU, XTT and confocal microscopy. Statistics were performed by one-way Anova, Tukey's tests and Pearson's correlation analysis at a pre-set significance level of 5 %.

Results. Raman mappings revealed coverage yield of 82 % for TiGS and ≥99 % for TiGD and TiGV. Both TiGD and TiGV presented FWHM > 44 cm^{-1} and I_D/I_G ratio < 0.12, indicating multiple graphene layers and occlusion of defects. The contact angle was significantly higher for TiGD and TiGV (110° and 117°) comparing to the Control (70°). The SFE was lower for TiGD (13.8 mN/m) and TiGV (12.1 mN/m) comparing to Control (38.3 mN/m). TiGD was selected for biofilm assays and exhibited significant reduction in biofilm formation for all microorganisms compared to Control. There were statistical correlations between the high contact angle and low SFE of TiGD and decreased biofilm formation.

Significance. TiGD presented high quality and coverage and decreased biofilm formation for all species. The increased hydrophobicity of graphene films was correlated with the decreased biofilm formation for various species.

* *Corresponding author at*: Faculty of Dentistry, Oral Sciences, National University of Singapore, 9 Lower Kent Ridge Road, Singapore.
E-mail address: denvr@nus.edu.sg (V. Rosa).

https://doi.org/10.1016/j.dental.2018.09.016
0109-5641/

1. Introduction

Peri-implantitis affects up to 20% of individuals with implants [1]. The disease results from a dysbiotic relationship of pathogenic microorganisms in biofilms accumulated on the surface of implants and the host tissues inducing progressive bone loss [2]. Biofilms are surface-attached, matrix-encased, structured microbial communities [3]. It is now known that at least 65% of all human infections, including peri-implantitis, are caused by microorganisms in the biofilm mode of growth [4]. During the sequence of biofilm formation on implants, the microbiota changes from the initial oral commensal bacteria to the highly pathogenic bacteria similar to the ones found in periodontal pockets of patients suffering from periodontitis [5,6]. In addition, *Candida albicans*, a major fungal pathogen, has been detected as an opportunistic species in peri-implant lesions. Thus, dental implants can be a potential reservoir for *C. albicans* associated infections [7].

The current treatment strategies for peri-implantitis include decontamination of the implant sites and infection control. Previous studies using non-chemical methods such as treatment with laser, ultrasound and air abrasion to reduce pathogenic bacterial counts have not produced promising results [8,9]. On the other hand, surgical procedures (*e.g.*, implantoplasty and guided tissue regeneration) are more effective in controlling established peri-implantitis lesions. However, these procedures are costly and demand long maintenance phase [10,11]. Adjunct therapies with antiseptics and systemic antibiotics have also not been very successful in improving clinical and microbiological parameters in peri-implant disease [12,13]. Moreover, pathogens isolated from the biofilms of peri-implantitis patients have demonstrated resistance to therapeutic concentrations of amoxicillin, clindamycin and other antibiotics under *in vitro* conditions [14]. Hence, the development of materials that reduce the adherence and biofilm formation of oral pathogenic bacteria and fungi on implant surfaces will be vital to minimize the oral and systemic infections associated with dental implants [7,15].

Dental implants made of titanium do not possess antibacterial properties. Therefore, a number of surface coatings methods have been developed to improve their antibacterial properties [16]. Although silver-based coatings have shown to improve general antibacterial activity on titanium, they are not specific in damaging bacterial cells, and are susceptible to oxidative dissolution and corrosion [17–19]. Combinations of antibiotics with chitosan or hydroxyapatite have potential to prevent infection on titanium [20,21]. However, development of antibiotic resistance is a concern in this approach. In addition, unfavourable mechanical properties of these materials, and lack of optimal release kinetics [22] warrants further studies on anti-biofilm surface coatings.

Graphene is an atom-thick layer of carbon atoms that can impact several dental biomedical applications [23]. It can be used as cytocompatible substrates and scaffolds to induce spontaneous osteoblastic differentiation and mineralization [24–27]. Moreover, graphene and its derivatives have shown promising anti-bacterial effects. The addition of graphene dispersed in poly(vinyl alcohol) matrix was capable to disrupt the growth of *Escherichia coli (E. coli)* and *Staphylococcus aureus* [28]. Graphene oxide decreases bacterial viability possibly due to physical disruption and chemical oxidation (*e.g.*, membrane stress and ROS-independent oxidative stress [29,30]). Remarkably, atom-thick graphene film emerges as a promising coating. It can be deposited onto full-sized dental implants and other three-dimensional orthopedic parts such as locking and compression plates [31]. Moreover, graphene film can prevent bacterial growth [32]. The reasons for such antibacterial effects remain largely unknown. One of the theories, the facile transfer of electrons from microbial membranes to graphene on conductive substrates, has been disproved [33]. Hence, understanding the mechanisms underlying the antibiofilm potential of graphene can lead to the development of the next-generation of implants, less susceptible to infections. The objective of this work was to evaluate the surface characteristics *viz.* coverage, number of layers, and superficial characteristics of a graphene film on titanium that render promising antimicrobial properties against oral bacterial and fungal pathogens. The hypothesis was that graphene inhibits biofilm proliferation by decreasing surface free energy (SFE) of the titanium surface.

2. Materials and methods

2.1. Sample preparation

Medical grade 4 titanium discs (Control, 12 mm diameter, 1 mm thick, Vulcanium, USA) were polished with silicon carbide paper (up to 2500 p, 150 rpm, 20 N). Thereafter, the samples were washed in ultrasonic bath with acetone, isopropanol and deionized water (20 min each).

Graphene was grown by single operator using a custom-built furnace in a Class 1000 clean room facility at the NUS Centre for Advanced 2D Materials and Graphene Research Centre as previously described [24]. The graphene film was transferred onto the discs using the vacuum assisted transfer technique. Firstly, the graphene coated copper foil was covered with polydimethylsiloxane (PDMS, Sylgard 184, Dow Corning Corporation, USA), spin coated at 1000 rpm and cured (135 °C, 20 min). A polyimide tape (3M, USA) was placed on top of the PDMS and the copper foil was etched away in a 1.5% ammonium persulfate solution. The transfer tape (polyimide/PDMS/graphene) was washed in deionized water (2 h) and gently blow-dried with N_2. Afterwards, the transfer tape was placed onto the disc, positioned in between two prefabricated PDMS square molds and inserted in a vacuum-sealing pouch. The set was placed in a vacuum chamber (Fig. 1) and the pressure was reduced to 0.02 bar for 60 s. Thereafter, the PDMS molds were removed and the transfer tape was peeled off leaving the graphene over the disc (TiGS). Afterward, freshly prepared transfer tapes were used for double (TiGD) and five times transfers (TiGV). Additional control was created to evaluate the quality of the transfer by depositing graphene onto SiO_2 (285 nm thick) on Si wafer which is widely used for the detection and characterization of single and multiple layers of graphene [34].

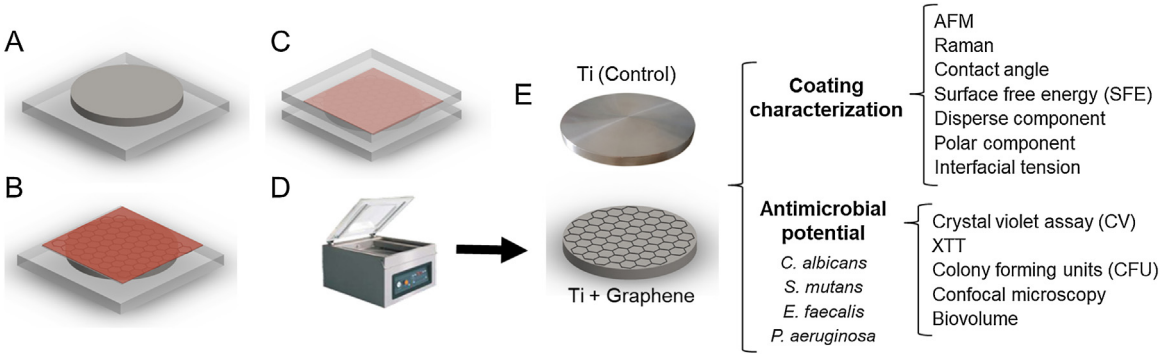

Fig. 1 – Process flow of graphene onto titanium disc by vacuum assisted dry transfer technique: (A) The titanium disc was placed on the prefabricated PDMS mold; (B) graphene/PDMS/polyimide tape was positioned in contact with the disc; (C) PDMS mold was placed on B; (D) The set (as shown in C) was inserted in a vacuum sealing bag and placed in the vacuum sealer chamber and the PDMS/polyimide tape eventually peeled off; (E) The uncoated titanium (Control) and graphene coated groups were characterized for surface characteristics, wettability and antibiofilm potential.

2.2. *Surface characterization: Raman spectroscopy, atomic force microscope and wettability*

Ten samples of each group were subjected for Raman (Raman Microscope CRM 200, Witec, Germany) and atomic force microscope (AFM, Bruker AXS, Germany) characterization. To evaluate the quality and coverage of the graphene coating, Raman spectrum for G (~1580 cm^{-1}), D (~1354 cm^{-1}) and 2D peaks (2680 cm^{-1}) were acquired (10 mappings per sample) as previously described [25]. Surface topography and roughness were analysed using tapping mode AFM with a silicon nitride tip (resonance frequency: 40–90 kHz: spring constant 0.4 N/m).

The contact angle measurements were determined at room temperature by dispensing 15 μl droplet of deionized water onto the surface of the samples (n = 5, 10 readings per sample, Drop Shape Analyzer DSA25, Kruss GmbH, Germany). The SFE, polar and non-polar components were obtained using the Owens, Wendt, Rabel and Kaelble (OWRK) method (Table 2 [35]).

2.3. *Microbial culture and biofilm formation*

Three bacterial strains (gram positive: *Streptococcus mutans UA159* and *Enterococcus faecalis ATCC 29212;* gram negative: *Pseudomonas aeruginosa* PAO1) and one fungal strain (*C. albicans SC5314*) were used for the study. For routine use, *S. mutans* and *E. faecalis* were subcultured on brain heart infusion (BHI) agar (Sigma-Aldrich, USA) and *P. aeruginosa* was subcultured on nutrient agar. *C. albicans* was subcultured on Glucose minimal medium (GMM) agar. *S. mutans* and *E. faecalis* were inoculated in BHI broth and *P. aeruginosa* was inoculated in nutrient broth and incubated for 16 h at 37 °C in an orbital shaker incubator at 80 rpm. Microbial cultures were then centrifuged at 5000 rpm for 5 min at 4 °C. Thereafter, the pellets were re-suspended in 1 ml of new medium and optical density (OD) was adjusted to 0.5 to 0.6 at a wavelength of 600 nm (approx. 10^7 cells/ml).

Similarly, *C. albicans* was taken from GMM agar plates, inoculated and grown in GMM medium and adjusted to an optical density of 0.375 to 0.385 at a wavelength of 520 nm (approx. 10^7 cells/ml).

2.4. *In vitro biofilm formation*

Biofilm formation was carried out in pre-sterilized, polystyrene, flat-bottomed, 24 well microtiter plate (Greiner bio-one, Singapore) as previously described [36]. The titanium disks were placed inside each well (n = 3) and washed with PBS and dried.

The disks were completely immersed in 1 ml of the OD adjusted cell suspensions. The biofilm was allowed to develop for 24 h at 37 °C in an orbital shaker incubator at 80 rpm.

2.5. *Crystal violet assay*

Crystal violet (CV) assay [37] was performed to quantify the total biofilm biomass of *S. mutans, E. faecalis, and P. aeruginosa*, respectively. After 24 h, the biofilms were washed gently with PBS applied on the side wall of the well to remove the non-adherent cells. Further, biofilms were fixed with 2% formalin at room temperature for 15 min. Subsequently, the discs were transferred to new wells, after which 1 ml of 1% crystal violet stain (Sigma-Aldrich) was added into each well for 5 min and then washed three times with PBS to remove the excess stain. Subsequently, 500 μl of 95% ethanol was added into each well and incubated for 15 min. After incubation 200 μl of ethanol was transferred to a new 96 well plate (Greiner bio-one, Singapore). The absorbance was measured at 570 nm using a spectrophotometer (Multiskan GO, Thermo Scientific, USA).

2.6. *XTT reduction assay*

XTT assay was performed to evaluate the metabolic activity of *C. albicans* as described previously [38]. After 24 h, the biofilms were washed gently with PBS applied on the side wall of the well to remove the non-adherent cells and the discs were transferred to new wells. Subsequently, 1 ml of

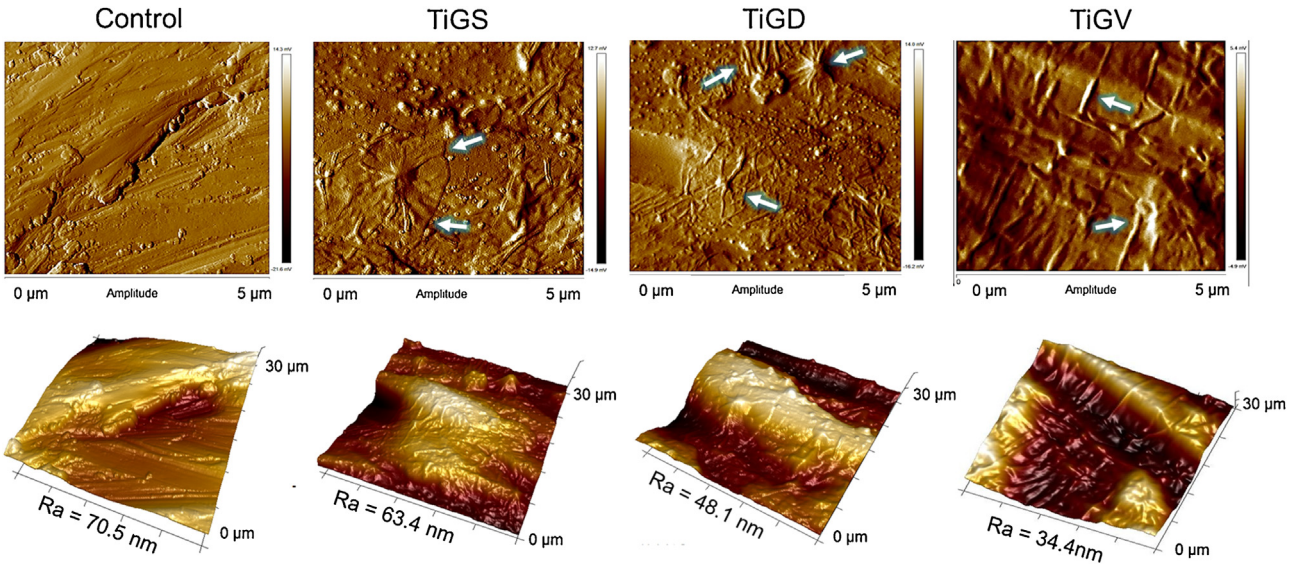

Fig. 2 – AFM micrographs of grade 4 titanium (Control), after single (TiGS), double (TiGD) and five graphene transfers (TiGV). Graphene folds (white arrows) can be observed on the TiGS, TiGD and TiGV (scale is 5 µm).

XTT-menadione solution was added into each well. Following incubation in dark at 37 °C for 20 min, 200 µl of solution was transferred to a 96 well plate and the colorimetric changes were measured by using a spectrophotometer at 490 nm.

2.7. *Colony forming unit assay (CFU)*

For colony forming units (CFU) counting, the biofilms formed over 24 h were washed gently with PBS. Subsequently the discs were immersed in PBS and the attached biofilms were dissociated by vigorous agitation for 3 min. A dilution series was prepared in PBS for the cell suspensions obtained from the respective biofilms. A volume of 100 µl from each dilution was plated on BHI (for *S. mutans* and *E. faecalis*), nutrient agar (for *P. aeruginosa*) and GMM agar (for *C. albicans*) for enumeration. The bacterial and fungal plates were grown for 24 h at 37 °C and 30 °C respectively. The colonies were counted and the corresponding log CFU values were calculated.

2.8. *Confocal laser scanning microscopy (CLSM)*

All microbial biofilms grown on Control and TiGD for 24 h were imaged using confocal microscopy. The bacterial biofilms were stained with SYTO-9 (excitation/emission 485/498 nm) and propidium iodide (excitation/emission 535/617 nm). *C. albicans* biofilms were stained with calcofluor white (excitation/emission 365/435 nm) according to a previously described protocol [39]. Stained biofilms were visualized using confocal microscope (Fluoview FV1000 TIRF, Olympus, Japan) and three-dimensional reconstructions obtained. Five random fields were analysed, and Z sections were reconstructed from three biological replicates for the quantification of the biovolume (Imaris 9.1, Bitplane AG, Switzerland).

2.9. *Statistical analysis*

All groups had three biological samples and the experiments were performed in independent triplicates. Shapiro–Wilk and Lavene's tests were performed for checking normality and homogeneity. One-way ANOVA and Tukey's test were used to analyze the data pertaining the wetting properties and microbial assays. Pearson's correlation analysis was used to determine the correlation between the microbial measurements (CV assay and CFU) and material properties (contact angle and SFE). A pre-set significance level of 5% was considered for all tests.

3. Results

3.1. *Graphene coated titanium: surface and coverage characterization*

The surface of graphene coated samples presented folds and bundles (arrows) and lower Ra with the increase in graphene transfers (Fig. 2). The Raman mappings revealed a coverage yield of 82% on TiGS and ≥99% for TiGD and TiGV (Table 1 and Figs. 3 and 4). Notably, the I_D/I_G ratio (indicative of defects) decreased with the increase of transfer procedures (Table 1).

The wetting characteristic are shown in Table 2. As approximately 20% of TiGS remained uncoated, the droplets

Table 1 – Surface coverage and characteristics of graphene transferred on grade 5 titanium *via* vacuum method after single (TiGS), double (TiGD) and five transfers (TiGV).

	Coverage (%)	FWHM	I2D/IG	I_D/I_G
TiGS	82.0	34.4	1.18	0.34
TiGD	99.1	44.1	1.26	0.12
TiGV	99.8	57.7	0.78	0.09

Table 2 – Wettability characterization of the groups tested. All the graphene coatings increased the hydrohobicity of grade 4 titanium. The results highlight the stronger hydrophobic trait of the samples as more graphene transfers are performed (different superscript letters in the same row indicate significant differences, $p < 0.05$).

		Control	TiGS	TiGD	TiGV
Contact angle (°)	Water	70.2 (1.9)^{d}	92.7 (2.2)^{c}	110.4 (1.3)^{b}	117.3 (2.4)^{a}
	Glycerol	59.0 (4.0)^{c}	92.2 (4.1)^{b}	110.8 (1.3)^{a}	111.5 (4.0)^{a}
	Ethylene glycol	42.4 (1.6)^{c}	79.3 (0.7)^{b}	91.0 (4.6)^{a}	95.8 (4.6)^{a}
	Diiodomethane	54.4 (5.0)^{d}	73.3 (5.5)^{c}	80.9 (4.3)^{b}	91.7 (4.3)^{a}
Surface free energy (mN/m)		38.3 (5.0)^{a}	18.1 (2.5)^{b}	13.8 (1.6)^{c}	12.1 (2.8)^{c}
Disperse component (mN/m)		28.9 (3.1)^{a}	14.3 (1.4)^{b}	12.6 (1.2)^{b}	11.7 (2.6)^{b}
Polar component (mN/m)		9.4 (1.9)^{a}	3.8 (1.0)^{b}	1.7 (0.4)^{c}	0.27 (0.1)^{c}
Interfacial tension (mN/m)		17.2 (1.3)^{d}	28.0 (4.9)^{c}	37.9 (7.2)^{b}	46.4 (4.1)^{a}

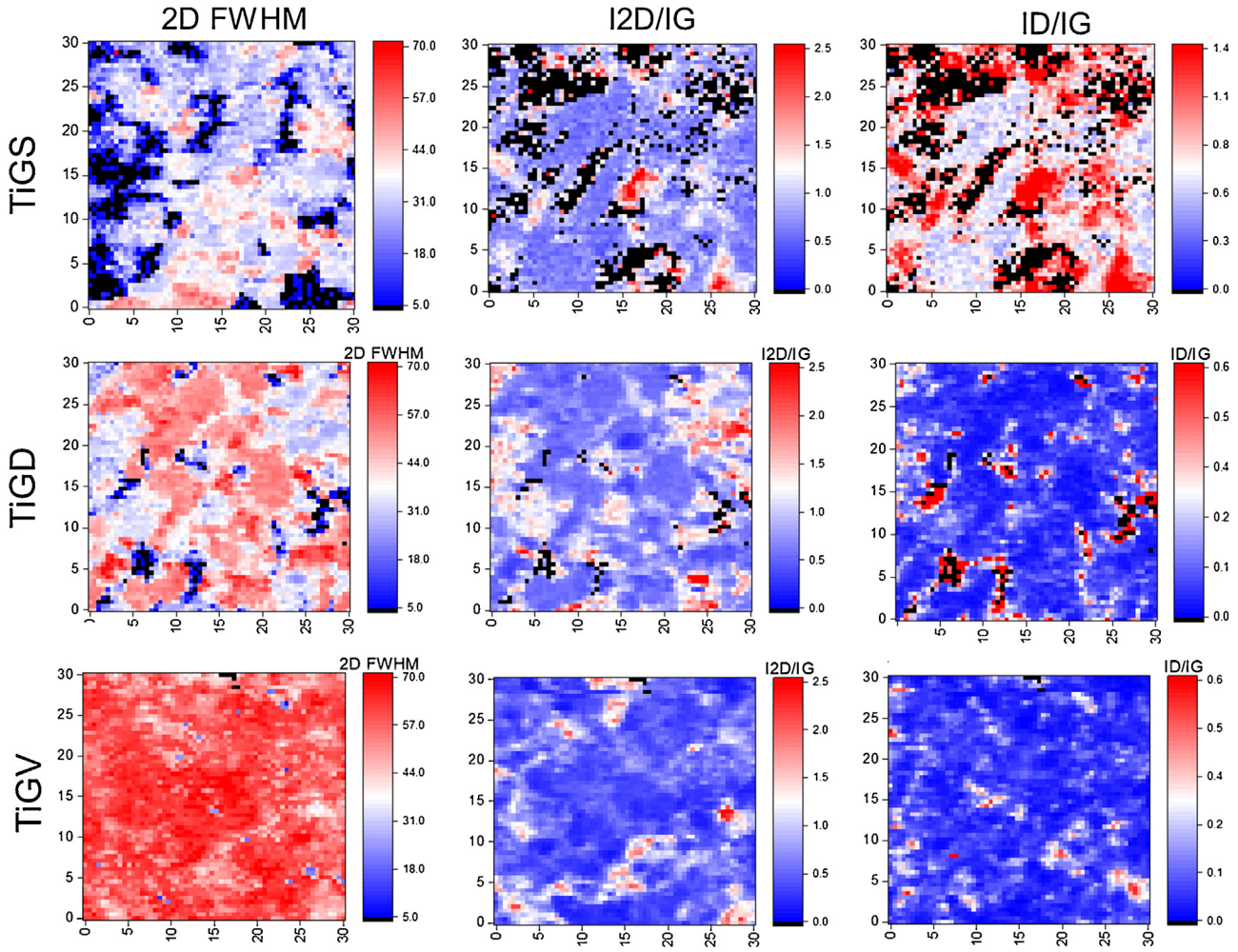

Fig. 3 – Raman characterization of graphene coated on titanium by vacuum assisted dry transfer. The analyses of FWHM (cm^{-1}) and I_{2D}/I_G indicate the increase in the number of graphene layers in TiGD and TiGV as compared to TiGS. I_D/I_G ratio demonstrates a prominent overall decrease in defect distribution in TiGD and TiGV compared to TiGS (black pixels indicating absence of graphene, mappings scale in μm).

were deposited on areas fully coated with graphene. There were significant increases in contact angles for all liquids on the graphene-coated specimens compared to the Control ($p < 0.05$). Also, there were significant decreases in the SFE and increases in the interfacial tension with the increase in number of graphene transfers ($p < 0.05$).

Finally, as the single transfer covered only ~80% of the sample surface, the TiGS group was excluded from further microbiological analysis.

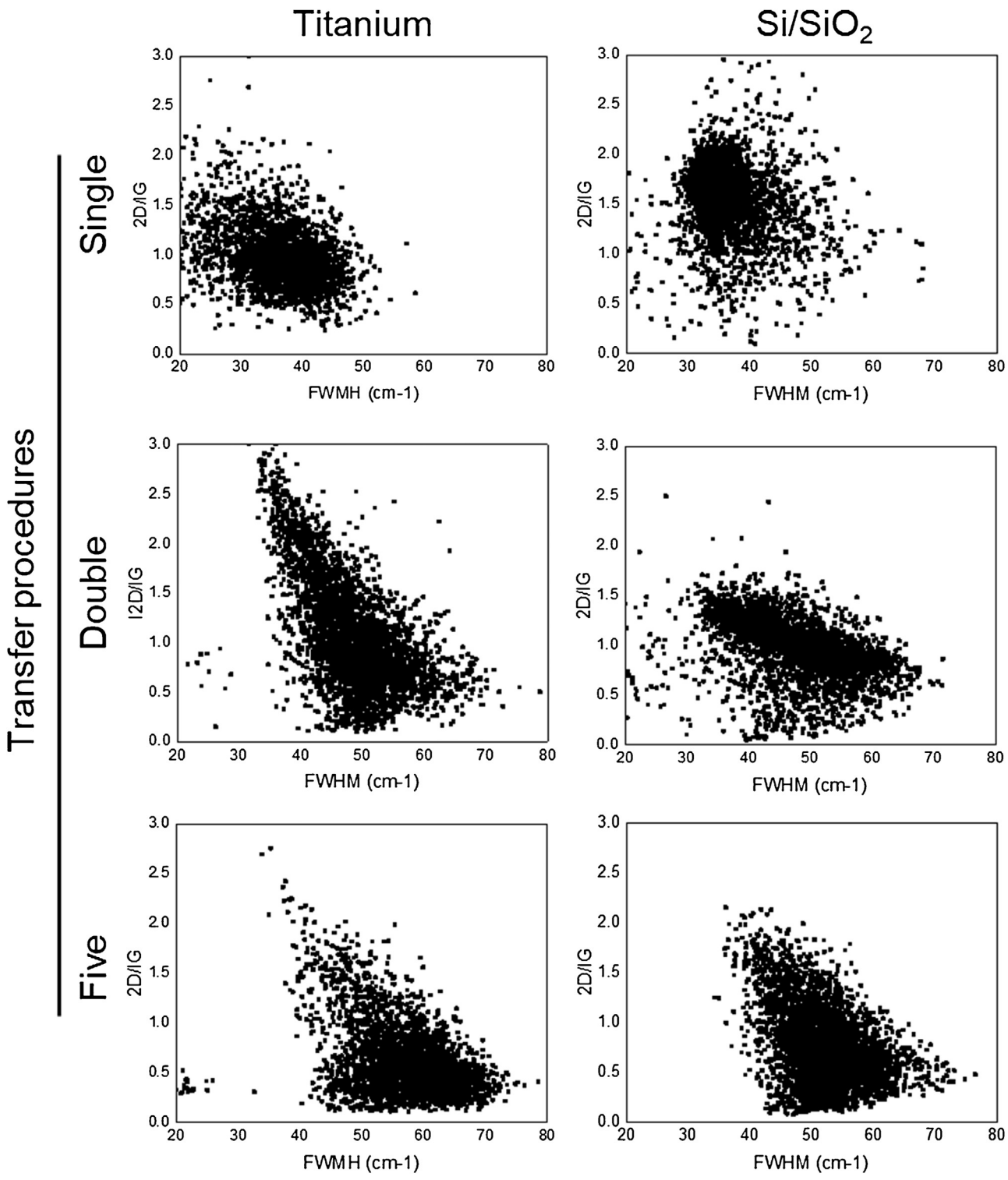

Fig. 4 – The scatter plots of I_{2D}/I_G-FWHM obtained on titanium reflect the morphological changes with the different transfers respectively had similar pattern compared to those obtained for graphene transferred onto SiO_2 wafer.

3.2. *Biofilm quantification*

CV assay and CFU showed significant decreases in both *C. albicans* and *S. mutans* when cultured on the graphene-coated specimens as compared to the Control (Fig. 5, $p < 0.05$). However, the increase in number of graphene layers (TiGV) failed to decrease further the microbial growth and number of CFUs ($p > 0.05$). Hence, only the antibacterial potential of TiGD was evaluated for *E. faecalis* and *P. aeruginosa*. Notably, TiGD had significantly decreased the biofilm accumulation for all species tested compared to the Control ($p < 0.05$).

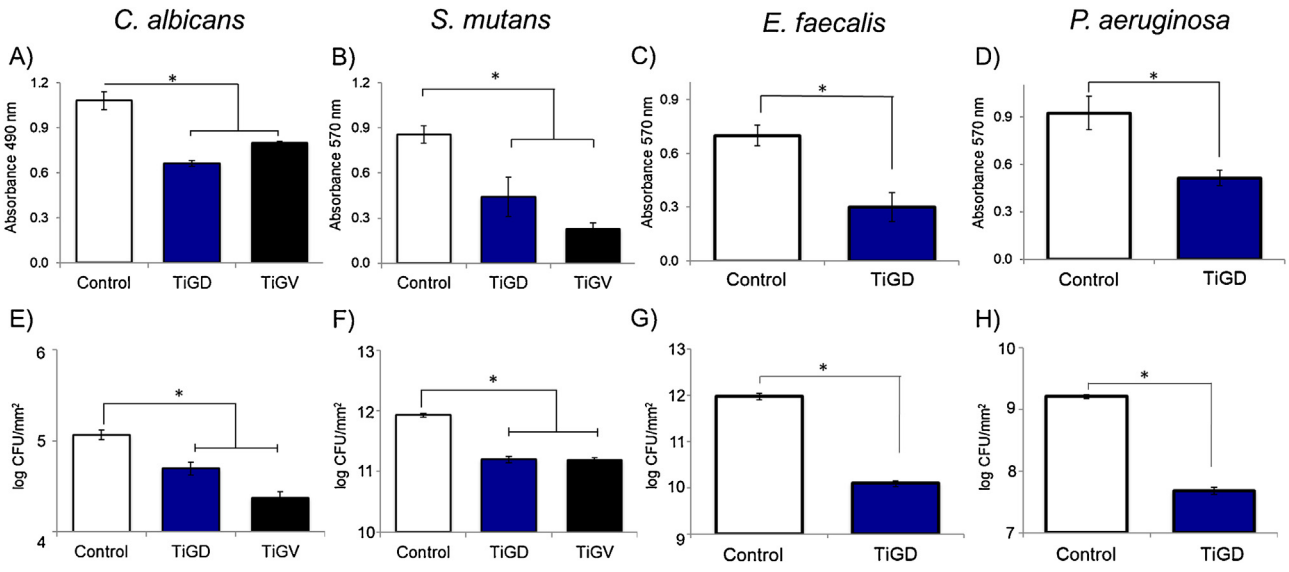

Fig. 5 – Graphene coated titanium (TiGD and TiGV) presented lesser microbial (bacterial and fungal) biofilm formation compared to the Control. XTT assay was used for quantifying *C. albicans* biofilm formation (A) and CV assay was used for evaluating the bacterial biofilms (B–D). TiGD or TiGV presented significant reductions in the number of total CFU (E–H. * denotes statistical difference, $p < 0.05$).

The CLSM revealed less biofilm formation of all bacterial species on TiGD compared to Control (Fig. 6). For *C. albicans*, TiGD reduced the biofilm formation and hyphal growth while the Control presented the typical architecture of cells bundled together with intermittent hyphal distribution (red arrows in Fig. 6, $p < 0.05$ for biovolume).

The Pearson's correlation analysis confirmed a correlation for increased contact angle and decreased SFE with respect to lower microbial quantification (Table 3).

4. Discussion

Anti-adhesive coating is one of the most promising strategies to reduce biofilm formation on implant surfaces [16]. Herein, we have successfully decreased the accumulation of gram-positive, gram-negative and fungal biofilms on titanium by coating its surface with graphene films.

We have succesfully deposited graphene onto titanium without the use of liquids and hazardous chemicals during the transfer procedure. The surface of the coated samples presented folds and bundles (Fig. 2) indicative of the presence of graphene [31]. The folds are attributed to the transfer tape that adapts to the substrate topography at a nanometric scale decreasing the roughness by only 36 nm after five transfers. TiGS presented a coverage yield of 82% (Table 1) that was lower than the one obtained by the hot-pressing method (>90%) for a single transfer step [32]. Nonetheless, the repetition of the transfer procedure increased the coverage area to 99% (Fig. 3 and Table 1). TiGS presented a FWHM of 34.4 cm^{-1} that is closer to the characteristic of single layer whereas the values for TiGD and TiGV were $\geq$44.1 cm^{-1} that are consonant with increased number of graphene layers [40]. TiGD and TiGV presented lower I_D/I_G ratio compared to TiGS confirming the occlusion of the defective areas [41]. The reliability of the transfer technique was confirmed on SiO_2 on Si wafer. The similar patterns observed in the scatter plots (Fig. 4) confirm that the titanium does not influence negatively the integrity and quality of graphene when this technique is employed.

The Raman characterization showed high quality, homogeneous and continuous graphene coverage on the titanium discs (Fig. 3). Previous publications have shown that CVD-grown graphene can be deposited on metals [31,42] and full-sized dental implants [31] and that the coating keeps its characteristics upon exposure to water, biomolecules and human cells [31,43]. The nature of interactions between graphene and titanium and other metals are not entirely known. In fact, chemisorbed metals interact with graphene by forming a chemical bond whereas on the physiosorbed metals no chemical bonding is formed [44,45]. Recent studies have shown that the interactions between graphene films and titanium (pure and grade 5 titanium alloy) result in a red shift of the 2D and G peaks [31,46]. Hence, it is possible that the titanium atoms diffuse at the surface of graphene creating bonds with the carbon atoms under them or occupying carbon atom vacancies [46].

Subsequently, we investigated the wetting characteristics (Table 2). Previous study suggested that graphene does not alter solid-liquid interactions regardless of the background substrate [47] while other affirmed that such effect breaks down depending on the material on which graphene is deposited [48]. Here, the contact angles of graphene-coated titanium were higher than the Control and similar to those observed for graphene on other substrates [49]. This suggests that graphene can subdue the hydrophilicity of the underlying substrate. Furthermore, the concomitant increase in hydrophobicity with number of transfers can be related to (i)

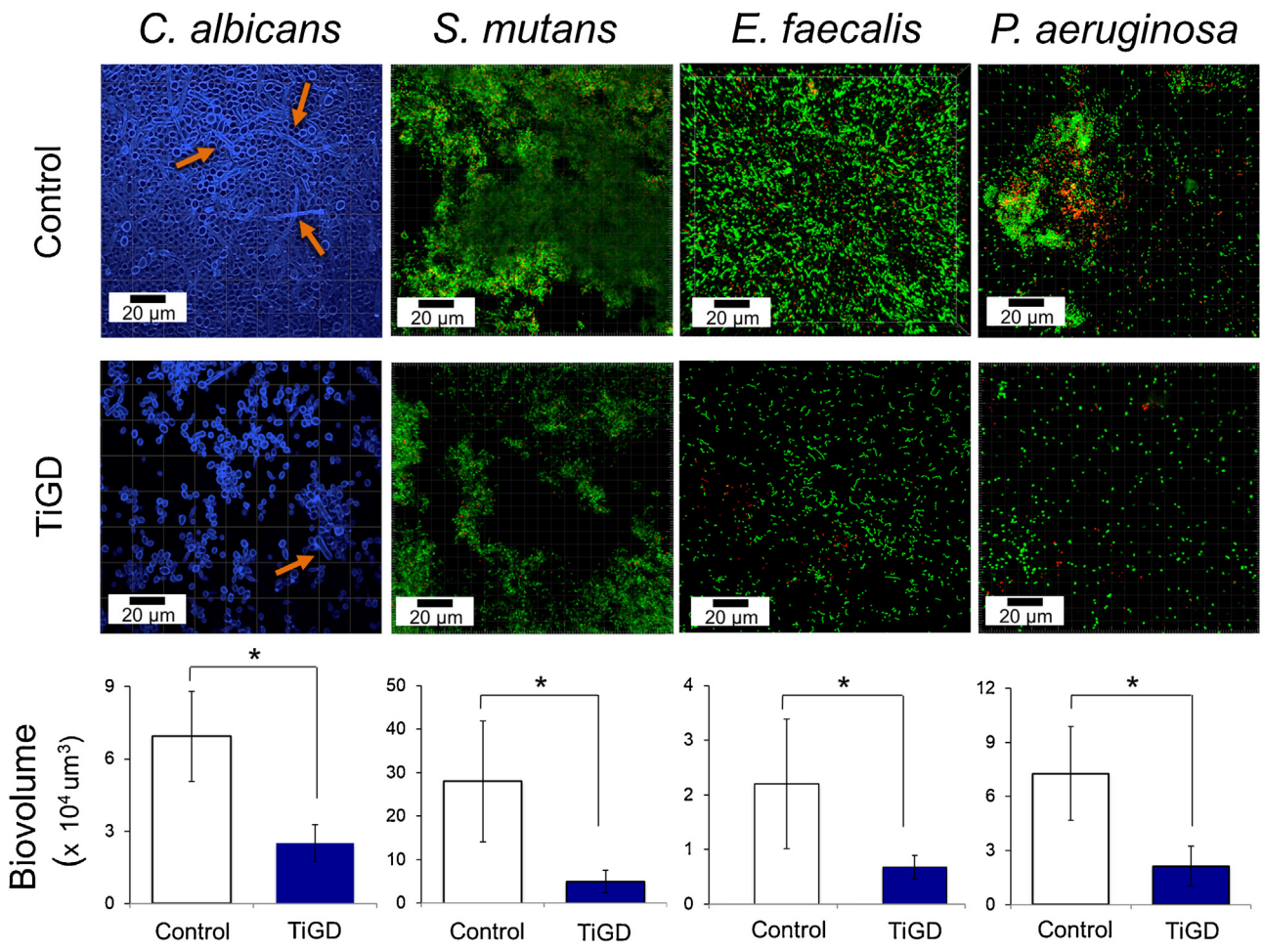

Fig. 6 – Biofilm formation. Biofilms were stained with SYTO-9 (green) and propidium iodide (red) and imaged with CLSM. The images revealed that TiGD decreased biofilm formation for all microorganisms tested. *C. albicans* biofilms exhibited limited hyphal occurrence (arrows) on TiGD compared to the typical bundled biofilm with hyphal formation on the Control. Moreover, there were less biofilm formation on TiGD for *S. mutans*, *E. faecalis* and *P. aeruginosa* compared to the Control. Note the significant (*) reduction of biovolume represented on the bar graph on TiGD for all the microbial species tested ($p < 0.05$). (for interpretation of the references to colour in this figure legend, the reader is referred to the web version of this article).

Table 3 – Pearson's correlation coefficient describing the relationship between material properties and microbial biofilm formation. The coefficients highlight the effects of high contact angle and low SFE on decreased biofilm formation (CV assay and CFU).

	Contact angle (°)			
	CVA		CFU	
	Pearson's r	p-Value	Pearson's r	p-Value
C. albicans	−0.6679	0.0493	−0.9708	0.0013
S. mutans	−0.9453	0.0001	−0.9768	0.0008
E. faecalis	−0.9423	0.0049	−0.9856	0.0144
P. aeruginosa	−0.9882	0.0015	−0.9983	0.0017
	Surface free energy (SFE, mN/m)			
	CVA		CFU	
	Pearson's r	p-Value	Pearson's r	p-Value
C. albicans	0.6811	0.0434	0.9840	0.0004
S. mutans	0.8483	0.0038	0.9578	0.0422
E. faecalis	0.9791	0.0006	0.9913	0.0001
P. aeruginosa	0.9712	0.0058	0.9994	0.0006

the occlusion of defects that brings homogeneity on the surface (Fig. 3 and Table 2) hampering the direct interaction of the liquids with the supporting substrate [50], and (ii) the decrease in I_D/I_G ratio (Table 1) which relates to higher interaction of graphene with the substrate or vacancies, decreasing both the polarity and the SFE [51,52].

C. albicans have been identified in 10 to 31% of peri-implantitis sites and may be associated with implant failure [6,53,54]. TiGD decreased the total CFU counts and the biovolume for *C. albicans* comparing to the Control. Moreover, the decreased hyphae formation on TiGD (arrows in Fig. 7) may indicate a potential of using a TiGD to decrease *C. albicans* virulence. A previous study that showed that lowering titanium SFE from 46 to 38 mN/m reduced *C. albicans*' CFU counts by 73% [55]. As the surface roughness was kept at the nanometric scale (Fig. 2), the decreases may be related to the low SFE of the graphene coatings (Table 2). In fact, there were statistical correlations between the lower SFE of TiGD and TiGV and decreases in total CFU (Table 3).

S. mutans and *E. faecalis* accumulate on the surface of implants *in vivo* and have been identified in high quantities in the peri-implant environment of diseased implants [56,57]. Likewise, gram-negative rods (*e.g., Pseudomonas spp.* and *Klebsiella spp.*) have been identified at heavy growth mode in increased number of patients with peri-implantitis [53,58]. *P. aeruginosa* exhibits extremely drug-resistant phenotypes and some of the strains are resistant to all types of antipseudomonal agents except polymyxins [59]. Notably, TiGD presented great potential to decrease early biofilm formation from these gram-positive and gram-negative bacterial strains (Figs. 5 and 6).

Bacteria can effectively adhere to materials with a degree of hydrophilicity (water contact angle of 40–70°) [60] like our Control (Table 2). Furthermore, several bacterial cell walls present high SFE that hamper their adherence to hydrophobic surfaces with reduced SFE [61–63]. Previously, coatings with SFE in the range of 21–29 mN/m have reduced *E. coli* adhesion by 68 to 94% [64]. Likewise, pyrolytic carbon valve models with low SFE (31 mN/m) presented less counts of *P. aeruginosa* compared to valve with SFE of 41 mN/m [65]. Moreover, lowering the titanium SFE decreased bacterial colonization and delayed biofilm maturation *in vivo* [66]. Hence, the decreases in biofilm accumulation observed on TiGD (Figs. 5 and 6) can be related to the significantly lower SFE provided by the coating (13.8 mN/m) compared to the Control (38.3 mN/m). There were statistical correlations between the SFE and contact angles and bacterial biofilm formation (Table 3) to confirm this hypothesis. In addition, the polar component of TiGD (1.7 mN/m) may contribute to the lower attachment of the bacteria and fungi onto the coated surfaces since low polar component (5 mN/m) decreases protein adherence [67].

Despite of having the lowest SFE (Table 2), TiGV failed to promote significant decrease in the biofilm formation for *S. mutans* and *C. albicans* compared to TiGD (Fig. 5). This suggests that once a homogenous graphene coating on titanium is established, changes in SFE of the graphene coating may be irrelevant to microbial interaction. In fact, previous studies have shown that each material present an optimum range of SFE in which the absorption and adhesion of specific proteins and bacteria are significantly decreased [68,69].

Despite the promising results, this work has some limitations. Although the study exhibits a robust antimicrobial potential of graphene, it is in a single species scenario. Therefore, further research is warranted to explore the effect of graphene on mixed microbial communities over time. However, the graphene coated titanium has potential to decrease microbial biofilm formation. This new technique may have an edge over other traditional coatings as it does not rely on antibiotics, is chemically stable, cytocompatible and can be successfully applied onto dental implants without the use of hazardous chemicals [24,25,31]. Future studies are needed to evaluate the extent of the antibiofilm potential of graphene compared to the existing alternatives under both *in vitro* and *in vivo* conditions.

5. Conclusion

CVD-grown graphene was successfully transferred on titanium *via* a dry transfer technique without the use of hazardous chemicals with a high-quality homogeneous coverage area of 99% and above. The hydrophilicity of titanium was strongly affected by the presence of the graphene coating. The graphene coatings decreased biofilm formation of bacterial and fungal species on titanium. However, there was no further significant change in the SFE and polar component after two graphene transfers. The high contact angle, low SFE and polar components of the graphene coating are the possible contributory factors that decreased biofilm formation.

Acknowledgements

The authors want to acknowledge Ms. Sim Yu Fan for the statistical support provided. The authors have no other relevant affiliations or financial involvement with any organization or entity with a financial interest in or financial conflict with the subject matter or materials discussed in the manuscript. This research was supported by the National Research Foundation, Prime Minister' Office, Singapore, under its Medium Sized Centre Program and by the grants from the Singapore Ministry of Education, Singapore (Academic Research Fund Tier 1, R-221-000-091-112, VR), National University Health System, Singapore (NUHS Open Collaborative Research Grant NUHS O-CRG 2016 Oct-25, NUHS Seed Grant Call FY2018 Sep-07, VR) and National Medical Research Council Singapore (NMRC/CIRG/1408/2014, CJS).

REFERENCES

[1] Mombelli A, Müller N, Cionca N. The epidemiology of peri-implantitis. Clin Oral Implants Res 2012;23:67–76.
[2] Faveri M, Figueiredo LC, Shibli JA, Pérez-Chaparro PJ, Feres M. Microbiological diversity of peri-implantitis biofilms. Adv Exp Med Biol 2015;830:85–96.
[3] Seneviratne CJ, Wang Y, Jin L, Wong SSW, Herath TDK, Samaranayake LP. Unraveling the resistance of microbial biofilms: has proteomics been helpful? Proteomics 2012;12:651–65.

[4] Potera C. Biofilms invade microbiology. Science 1996;273:1795–7.
[5] Hultin M, Gustafsson A, Hallstrom H, Johansson LA, Ekfeldt A, Klinge B. Microbiological findings and host response in patients with peri-implantitis. Clin Oral Implants Res 2002;13:349–58.
[6] Leonhardt A, Renvert S, Dahlen G. Microbial findings at failing implants. Clin Oral Implants Res 1999;10:339–45.
[7] Burgers R, Hahnel S, Reichert TE, Rosentritt M, Behr M, Gerlach T, et al. Adhesion of *Candida albicans* to various dental implant surfaces and the influence of salivary pellicle proteins. Acta Biomater 2010;6:2307–13.
[8] Persson GR, Samuelsson E, Lindahl C, Renvert S. Mechanical non-surgical treatment of peri-implantitis: a single-blinded randomized longitudinal clinical study. II. Microbiological results. J Clin Periodontol 2010;37:563–73.
[9] Persson GR, Roos-Jansaker AM, Lindahl C, Renvert S. Microbiologic results after non-surgical erbium-doped:yttrium, aluminum, and garnet laser or air-abrasive treatment of peri-implantitis: a randomized clinical trial. J Periodontol 2011;82:1267–78.
[10] Schwarz F, Sahm N, Becker J. Combined surgical therapy of advanced peri-implantitis lesions with concomitant soft tissue volume augmentation. A case series. Clin Oral Implants Res 2014;25:132–6.
[11] Mahato N, Wu X, Wang L. Management of peri-implantitis: a systematic review, 2010–2015. SpringerPlus 2016;5.
[12] Thone-Muhling M, Swierkot K, Nonnenmacher C, Mutters R, Flores-de-Jacoby L, Mengel R. Comparison of two full-mouth approaches in the treatment of peri-implant mucositis: a pilot study. Clin Oral Implants Res 2010;21:504–12.
[13] Hallstrom H, Persson GR, Lindgren S, Olofsson M, Renvert S. Systemic antibiotics and debridement of peri-implant mucositis. A randomized clinical trial. J Clin Periodontol 2012;39:574–81.
[14] Rams TE, Degener JE, van Winkelhoff AJ. Antibiotic resistance in human peri-implantitis microbiota. Clin Oral Implants Res 2014;25:82–90.
[15] Glavis-Bloom J, Vasher S, Marmor M, Fine AB, Chan PA, Tashima KT, et al. Candida and cardiovascular implantable electronic devices: a case of lead and native aortic valve endocarditis and literature review. Mycoses 2015;58:637–41.
[16] Wang Z, Shen Y, Haapasalo M. Dental materials with antibiofilm properties. Dent Mater 2014;30:e1–16.
[17] Imrell T. The importance of the thickness of silver coating in the corrosion behaviour of copper contacts; 1991. p. 237–43, http://dx.doi.org/10.1109/HOLM.1991.170829.
[18] Pokrowiecki R, Zareba T, Szaraniec B, Pałka K, Mielczarek A, Menaszek E, et al. In vitro studies of nanosilver-doped titanium implants for oral and maxillofacial surgery. Int J Nanomed 2017;12:4285–97.
[19] Kittler S, Greulich C, Diendorf J, Köller M, Epple M. Toxicity of silver nanoparticles increases during storage because of slow dissolution under release of silver ions. Chem Mater 2010;22:4548–54.
[20] Shi X, Wu H, Li Y, Wei X, Du Y. Electrical signals guided entrapment and controlled release of antibiotics on titanium surface. J Biomed Mater Res A 2013;101A:1373–8.
[21] Stigter M, Bezemer J, de Groot K, Layrolle P. Incorporation of different antibiotics into carbonated hydroxyapatite coatings on titanium implants, release and antibiotic efficacy. J Control Release 2004;99:127–37.
[22] Romanò CL, Scarponi S, Gallazzi E, Romanò D, Drago L. Antibacterial coating of implants in orthopaedics and trauma: a classification proposal in an evolving panorama. J Orthop Surg Res 2015;10.
[23] Xie H, Cao T, Rodriguez-Lozano FJ, Luong-Van EK, Rosa V. Graphene for the development of the next-generation of biocomposites for dental and medical applications. Dent Mater 2017;33:765–74.
[24] Xie H, Chua M, Islam I, Bentini R, Cao T, Viana-Gomes JC, et al. CVD-grown monolayer graphene induces osteogenic but not odontoblastic differentiation of dental pulp stem cells. Dent Mater 2017;33:e13–21.
[25] Xie H, Cao T, Gomes JV, Castro Neto AH, Rosa V. Two and three-dimensional graphene substrates to magnify osteogenic differentiation of periodontal ligament stem cells. Carbon 2015;93:266–75.
[26] Kalbacova M, Broz A, Kong J, Kalbac M. Graphene substrates promote adherence of human osteoblasts and mesenchymal stromal cells. Carbon 2010;48:4323–9.
[27] Dubey N, Bentini R, Islam I, Cao T, Castro Neto AH, Rosa V. Graphene a versatile carbon-based material for bone tissue engineering. Stem Cells Int 2015;2015:1–12.
[28] Ma Y, Bai D, Hu X, Ren N, Gao W, Chen S, et al. Robust and antibacterial polymer/mechanically exfoliated graphene nanocomposite fibers for biomedical applications. ACS Appl Mater Interfaces 2018;10:3002–10.
[29] Lu X, Feng X, Werber JR, Chu C, Zucker I, Kim JH, et al. Enhanced antibacterial activity through the controlled alignment of graphene oxide nanosheets. Proc Natl Acad Sci U S A 2017;114:E9793–801.
[30] Song C, Yang CM, Sun XF, Xia PF, Qin J, Guo BB, et al. Influences of graphene oxide on biofilm formation of gram-negative and gram-positive bacteria. Environ Sci Pollut Res Int 2018;25:2853–60.
[31] Morin JLP, Dubey N, Decroix FED, Luong-Van EK, Castro Neto AH, Rosa V. Graphene transfer to 3-dimensional surfaces: a vacuum-assisted dry transfer method. 2D Mater 2017;4:025060.
[32] Dubey N, Ellepola K, Decroix FED, Morin JLP, Castro Neto AH, Seneviratne CJ, et al. Graphene onto medical grade titanium: an atom-thick multimodal coating that promotes osteoblast maturation and inhibits biofilm formation from distinct species. Nanotoxicology 2018;12:274–89.
[33] Dellieu L, Lawarée E, Reckinger N, Didembourg C, Letesson JJ, Sarrazin M, et al. Do CVD grown graphene films have antibacterial activity on metallic substrates? Carbon 2015;84:310–6.
[34] Abergel DSL, Russell A, Fal'ko VI. Visibility of graphene flakes on a dielectric substrate. Appl Phys Lett 2007;91:063125.
[35] Kozbial A, Li Z, Conaway C, McGinley R, Dhingra S, Vahdat V, et al. Study on the surface energy of graphene by contact angle measurements. Langmuir 2014;30:8598–606.
[36] Ellepola K, Liu Y, Cao T, Koo H, Seneviratne CJ. Bacterial GtfB augments *Candida albicans* accumulation in cross-kingdom biofilms. J Dent Res 2017;96:1129–35.
[37] O'Toole GA. Microtiter dish biofilm formation assay. J Vis Exp 2011;47:2437.
[38] Seneviratne CJ, Jin LJ, Samaranayake YH, Samaranayake LP. Cell density and cell aging as factors modulating antifungal resistance of *Candida albicans* biofilms. Antimicrob Agents Chemother 2008;52:3259–66.
[39] Ellepola K, Liu Y, Cao T, Koo H, Seneviratne H. Bacterial GtfB augments *Candida albicans* accumulation in cross-kingdom biofilms. J Dent Res 2017, 22034517714414.
[40] Ferrari AC, Meyer JC, Scardaci V, Casiraghi C, Lazzeri M, Mauri F, et al. Raman spectrum of graphene and graphene layers. Phys Rev Lett 2006;97:187401.
[41] Dresselhaus MS, Jorio A, Souza Filho AG, Saito R. Defect characterization in graphene and carbon nanotubes using Raman spectroscopy. Philos Trans A Math Phys Eng Sci 2010;368:5355–77.
[42] Rodriguez CLC, Kessler F, Dubey N, Rosa V, Fechine GJM. CVD graphene transfer procedure to the surface of stainless steel for stem cell proliferation. Surf Coat Technol 2017;311:10–8.

[43] Velický M, Cooper AJ, Toth PS, Patten HV, Woods CR, Novoselov KS, et al. Mechanical stability of substrate-bound graphene in contact with aqueous solutions. 2D Mater 2015;2:024011.
[44] Giovannetti G, Khomyakov PA, Brocks G, Karpan VM, van den Brink J, Kelly PJ. Doping graphene with metal contacts. Phys Rev Lett 2008;101.
[45] Zheng J, Wang Y, Wang L, Quhe R, Ni Z, Mei WN, et al. Interfacial properties of bilayer and trilayer graphene on metal substrates. Sci Rep 2013;3:2081.
[46] Xu H, Wu X, Li X, Luo C, Liang F, Orignac E, et al. Properties of graphene-metal contacts probed by Raman spectroscopy. Carbon 2018;127:491–7.
[47] Rafiee J, Mi X, Gullapalli H, Thomas AV, Yavari F, Shi Y, et al. Wetting transparency of graphene. Nat Mater 2012;11:217–22.
[48] Shih CJ, Wang QH, Lin S, Park KC, Jin Z, Strano MS, et al. Breakdown in the wetting transparency of graphene. Phys Rev Lett 2012;109:176101.
[49] Wang S, Zhang Y, Abidi N, Cabrales L. Wettability and surface free energy of graphene films. Langmuir 2009;25:11078–81.
[50] Raj R, Maroo SC, Wang EN. Wettability of graphene. Nano Lett 2013;13:1509–15.
[51] Shin YJ, Wang Y, Huang H, Kalon G, Wee AT, Shen Z, et al. Surface-energy engineering of graphene. Langmuir 2010;26:3798–802.
[52] Ni ZH, Chen W, Fan XF, Kuo JL, Yu T, Wee ATS, Shen ZX. Raman spectroscopy of epitaxial graphene on a SiC substrate. Phys Rev B 2008;77:115416.
[53] Albertini M, Lopez-Cerero L, O'Sullivan MG, Chereguini CF, Ballesta S, Rios V, et al. Assessment of periodontal and opportunistic flora in patients with peri-implantitis. Clin Oral Implants Res 2015;26:937–41.
[54] Schwarz F, Becker K, Rahn S, Hegewald A, Pfeffer K, Henrich B. Real-time PCR analysis of fungal organisms and bacterial species at peri-implantitis sites. Int J Implant Dent 2015;1.
[55] Villard N, Seneviratne C, Tsoi JK, Heinonen M, Matinlinna J. *Candida albicans* aspects of novel silane system-coated titanium and zirconia implant surfaces. Clin Oral Implants Res 2015;26:332–41.
[56] Flanagan D. *Enterococcus faecalis* and dental implants. J Oral Implantol 2017;43:8–11.
[57] Nakazato G, Tsuchiya H, Sato M, Yamauchi M. In vivo plaque formation on implant materials. Int J Oral Maxillofac Implants 1989;4:321–6.
[58] Charalampakis G, Leonhardt Å, Rabe P, Dahlén G. Clinical and microbiological characteristics of peri-implantitis cases: a retrospective multicentre study. Clin Oral Implants Res 2012;23:1045–54.
[59] Ardila CM, Fernandez N, Guzman IC. Antimicrobial susceptibility of moxifloxacin against gram-negative enteric rods from colombian patients with chronic periodontitis. J Periodontol 2010;81:292–9.
[60] Lee JH, Khang G, Lee JW, Lee HB. Interaction of different types of cells on polymer surfaces with wettability gradient. J Colloid Interface Sci 1998;205:323–30.
[61] Uyen M, Busscher HJ, Weerkamp AH, Arends J. Surface free energies of oral streptococci and their adhesion to solids. FEMS Microbiol Lett 1985;30:103–6.
[62] Busscher HJ, Weerkamp AH, van der Mei HC, van Pelt AW, de Jong HP, Arends J. Measurement of the surface free energy of bacterial cell surfaces and its relevance for adhesion. Appl Environ Microbiol 1984;48:980–3.
[63] Teughels W, Van Assche N, Sliepen I, Quirynen M. Effect of material characteristics and/or surface topography on biofilm development. Clin Oral Implants Res 2006;17(Suppl 2):68–81.
[64] Zhao Q, Wang S, Müller-Steinhagen H. Tailored surface free energy of membrane diffusers to minimize microbial adhesion. Appl Surf Sci 2004;230:371–8.
[65] Litzler P-Y, Benard L, Barbier-Frebourg N, Vilain S, Jouenne T, Beucher E, et al. Biofilm formation on pyrolytic carbon heart valves: influence of surface free energy, roughness, and bacterial species. J Thorac Cardiovasc Surg 2007;134:1025–32.
[66] Quirynen M, Van der Mei HC, Bollen CM, Van den Bossche LH, Doornbusch GI, van Steenberghe D, et al. The influence of surface-free energy on supra- and subgingival plaque microbiology. An in vivo study on implants. J Periodontol 1994;65:162–7.
[67] Harnett EM, Alderman J, Wood T. The surface energy of various biomaterials coated with adhesion molecules used in cell culture. Colloids Surf B Biointerfaces 2007;55:90–7.
[68] McGuire J, Swartzel KR. The influence of solid surface energetics on macromolecular adsorption from milk. J Food Process Preserv 1989;13:145–60.
[69] Baier RE. Substrata influences on the adhesion of microorganisms and their resultant new surface properties. In: Bitton G, Marshall KS, editors. Adsorption of microorganisms. Hoboken: Wiley-Interscience Publishers; 1980. p. 59–104.